Effect of Sn Incorporation on the Thermal Transformation and Reducibility of M(II)Al-Layered Double Hydroxides [M(II) = Ni or Co]

S. Velu,[†] K. Suzuki,*[,†] M. P. Kapoor,[‡] S. Tomura,[†] F. Ohashi,[†] and T. Osaki[†]

Ceramics Technology Department, National Industrial Research Institute of Nagoya, 1-1 Hirate-cho, Kita-ku, Nagoya 462-8510, and Department of Energy and Environment, Osaka National Research Institute, 1-8-31, Midorigaoka, Ikeda, Osaka 563-8577, Japan

Received July 27, 1999. Revised Manuscript Received November 23, 1999

Our recent study on the incorporation of Sn in the lattice of MgAl-layered double hydroxides (LDHs) indicated that about 30 atom % of Al^{3+} could be isomorphously substituted by Sn^{4+} to form a new MgAlSn ternary LDH. In the present study, similar NiAlSn- and CoAlSn-LDHs were synthesized by a coprecipitation method. The influence of Sn on the thermal transformation and redox properties of NiAl- and CoAl-LDHs and their thermally derived products were investigated by X-ray powder diffraction (XRD), thermogravimetry/differential thermal analyses (TG/DTA), and temperature-programmed reduction (TPR) methods. The thermal transformation and reducibility of NiAlSn-LDH were different from that of the CoAlSn-LDH. Sn crystallized out as a SnO_2 phase along with NiO and $NiAl_2O_4$ phases from NiAlSn-LDH calcined above 900 °C. On the other hand, a mixture of nonstoichiometric Co-spinel and Co_2SnO_4 inverse spinel phases was noticed from CoAlSn-LDH. The TPR profiles of NiAl-LDH and its calcined products exhibited peaks for the reduction of Ni^{2+} species existing in different chemical environments while an additional peak for the reduction of $Sn^{4+} \rightarrow Sn^{o}$ was observed in the Sn-containing counterparts. The Sn incorporation greatly enhanced the reducibility of Ni-containing phases. The CoAl- and CoAlSn-LDH and their calcined products exhibited complex TPR profiles. At least three different reduction regions were identified. They were assigned to the reduction of $Co^{2+}-Co^{3+}$ (Co_3O_4-like) species (region I, between 250 and 450 °C), Co_3O_4-like species containing Al^{3+} or $CoAl_2O_4$-like species containing Co^{3+} (region II, 500−550 °C) and $Co^{2+}-Al^{3+}$ ($CoAl_2O_4$-like) species (region III, above 550 °C). In contrast to that observed in the Ni-containing analogues the reducibility of Co species in these samples was found to decrease upon Sn incorporation.

Introduction

Layered double hydroxides (LDHs), also known as anionic clays, are an important class of material currently receiving increasing interests owing to their potential applications as catalyst precursors and microporous materials.[1−3] They consist of positively charged brucite [$Mg(OH)_2$]-like M(II)−M(III) hydroxide layers which are separated from each other by an interlayer composed of anions and waters of crystallization. These compounds are represented by the general formula: $[M(II)_{1-x}M(III)_x(OH)_2]^{x+}[(A^{n-})_{x/n}\cdot mH_2O]^{x-}$, where M(II) is a divalent cation such as Mg, Cu, Ni, Co, Zn; M(III) is a trivalent cation such as Al, Fe, Cr, V, Mn, Ga, Rh; and A^{n-} is a charge-compensating anion such as CO_3^{2-}, NO_3^-, Cl^-, etc. There are mainly two classes of LDHs already known in the literature.[4,5] The class I LDHs are those containing various M(II)−M(III) cation pairs with different anions in the interlayer. Also, LDHs containing more than one M(II) cation and/or more than one M(III) cation in the layers have been reported. The class II LDH is obtained by the combination of M(I) and M(III) matrix cations (example, LiAl-LDH). It is also expected to synthesize a third class of LDH comprising M(II)−M(IV) cation pairs. For example, Taylor has reported the synthesis of a CoTi-LDH by an induced hydrolysis method.[6] However, it is unclear if the compound contained a single LDH phase as the detailed physicochemical properties of the material have not been described.

We have been attempting to synthesize M(II)−M(IV) LDHs by a coprecipitation method. We have shown recently the partial substitution of Al^{3+} by M(IV) cations such as Zr^{4+} in the MgAl-LDHs and their catalytic performance in the liquid-phase hydroxylation of phenol.[7,8] The incorporation of an another M(IV) cation, Sn^{4+}, in the M(II)Al-LDH matrix is being investigated

[†] National Industrial Research Institute of Nagoya.
[‡] Osaka National Research Institute.

(1) Cavani, F.; Trifiro, F.; Vaccari, A. *Catal. Today*. **1991**, *11*, 173.
(2) Trifiro, F.; Vaccari, A. In *Comprehensive Supramolecular Chemistry*; Atwood, J. L., Davies, J. E., MacNicol, D. D., Vögtle, F., Eds.; Pergamon: Elmsford, NY, 1997; Vol. 7, pp 251−291.
(3) Numerous examples for catalytic applications of LDH clays can be found in a special issue of *Appl. Clay Sci*. **1998**, *13*, 311−511.
(4) Newman, S. P.; Jones, W. *New J. Chem*. **1998**, *22*, 105.
(5) Vaccari, A. *Catal. Today* **1998**, *41*, 53.
(6) Taylor, M. *Clay Miner*. **1984**, *19*, 591.
(7) Velu, S.; Veda Ramasamy.; Ramani, A.; Chanda B. M.; Sivasanker, S. *Chem. Commun*. **1997**, 2107.
(8) Velu, S.; Sabde, D. P.; Shah, N.; Sivasanker, S. *Chem. Mater*. **1998**, *10*, 3451.

10.1021/cm9904685 CCC: $19.00
Published on Web 02/08/2000

currently. Our detailed study using XRD, SEM, FT-IR, and ^{119}Sn- and ^{27}Al-MAS NMR techniques indicated that about 30 atom % of the Al^{3+} in the brucite-like Mg−Al layer could be isomorphously substituted by Sn^{4+} to obtain a new MgAlSn ternary LDH.[9] Further increase in the concentration of Sn^{4+} resulted in the co-formation of a $MgSn(OH)_6$ phase along with the LDH phase. As a continuation of our study, we replaced the Mg^{2+} with Ni^{2+}/Co^{2+} in the Mg−Al−Sn−LDHs since LDHs containing transition metal ions such as Ni^{2+} or Co^{2+} are found to possess unique physicochemical properties for electrochemical, magnetic, and catalytic applications.[10,11] The synthesis of Sn-incorporated mesoporous zeolite-like materials has attracted much interest in recent years because of their potential applications in catalysis.[12,13] Several Sn-containing mixed-oxide systems have been widely employed as a powerful catalyst for a variety of organic trasformations.[14,15] It has been reported that the addition of Sn to Pt improved the catalytic performance of the re-forming reaction by an ensemble or ligand effect.[16] Ni-based catalysts containing small amounts of Sn were found to promote the steam re-forming of CH_4 with minimal formation of coke.[17] Hence, it is interesting, especially for catalytic applications, to investigate the effect of incorporation of Sn^{4+} in the layers of M(II)Al-LDHs with M(II) being Ni or Co on the structural and redox properties of the new materials.

Experimental Section

Synthesis of Sn-Incorporated LDHs. M(II)Al-LDHs and their Sn-incorporated analogues were synthesized by a coprecipitation method at room temperature by reacting aqueous solutions containing a mixture of $M(II)(NO_3)_2$ (M(II) = Ni or Co), $Al(NO_3)_3$, and $SnCl_4$ salts as precursors and a mixture of NaOH (∼2 M solution) and Na_2CO_3 (∼0.3 M solution) as precipitants at a constant pH (∼9).[9] The resulting precipitate was aged at 65 °C for 30 min with stirring in a magnetic stirrer, and then filtered, washed with deionized water several times until the pH of the filtrate was 7, and then dried in an air oven at 70 °C overnight.

Materials Characterization. The chemical compositions of the samples were determined by X-ray fluorescence (XRF) spectroscopy (Shimadzu Co. Lab center, XRF-1700 sequential X-ray fluorescence spectrometer). The powder X-ray diffraction (XRD) of the samples were recorded in the 2θ range 5−70° using Rigaku instruments equipped with a Ni-filtered Cu Kα radiation (λ = 1.5418 Å). The XRD patterns of all the as-synthesized samples were collected using a scan rate of 0.5° 2θ/min employing step scan mode with steps of 0.01° 2θ and a counting time of 1.2 s (instrument model: Rint 2100). For all the calcined samples the data were collected with a scan rate of 1° 2θ/min to calculate the lattice parameters, while a speed of 2°/min (step scan 0.02° 2θ) was used for obtaining the XRD patterns (instrument model: RAD-1 VC). In both cases, the observed interplanar "*d*" spacing was corrected using elemental Si as an internal standard [$d(111)$ = 3.1355 Å; JCPDS file no. 27-1402]. The crystallite sizes of the LDHs were calculated using Debye−Scherrer equation,[18] $t = 0.9\,\lambda/\beta \cos\theta$, where λ is the wavelength of the radiation (1.5418 Å), β is the line broadening of the peak due to small crystallites (rad 2θ) and θ, the corresponding angle of the diffraction peak. The full width at half-maximum (fwhm) of the (003) and (006) reflections of LDHs was measured for the calculation of crystallite sizes. A correction for instrumental broadening was also employed; $\beta = (B^2 - b^2)^{0.5}$, where "*B*" is the total broadening and "*b*" is the instrumental broadening. The instrumental broadening was determined by the measurement of the fwhm of the (113) reflection of α-Al_2O_3 (corundum) and the estimated value of b = 0.0021 rad 2θ. Simultaneous TG/DTA experiments were performed on a SSC/5200, SII Seiko instrument in the temperature range 50−700 °C in both N_2 and air atmospheres. A temperature ramp of 10 °C/min was employed.

The redox properties of the LDHs and their calcined products were investigated by temperature-programmed reduction (TPR) method. The experimental parameters were selected to meet the recommendations of Monti and Baiker.[19] About 50 mg of the sample was placed in a quartz reactor (i.d. 4 mm) and reduced in a stream of H_2 (5 vol % in Ar) at a heating rate of 5 °C/min up to 700 °C or in a few cases up to 800 °C. The hydrogen consumption due to the reduction of constituent cations was monitored continuously by a gas chromatograph (Shimadzu GC-8A) equipped with a thermal conductivity detector (TCD). The quantity of hydrogen consumed was calculated from the TPR peak area calibrated with a known amount of standard CuO sample (Wako Chemicals, Japan). For comparison, the TPR of reference samples such as SnO_2, CoO, and Co_3O_4 (Wako Chemicals, Japan) was also performed. A reference sample of $CoAl_2O_4$ was prepared by coprecipitation of $Co(NO_3)_2$ and $Al(NO_3)_3$ (1:2 molar ratio) using NH_4OH in the pH range 8−9 followed by calcination at 500 °C for 10 h. The TPR of this sample was used as a reference in the present study.

Results and Discussion

XRD of As-Synthesized Samples. The XRD patterns of NiAl-LDH, CoAl-LDH and their Sn-containing analogues are presented in Figure 1. It can be clearly seen that all the samples exhibit a single phase corresponding to the LDH. All the diffraction peaks within the 2θ range measured in the present study are sharp enough to calculate the lattice parameters more precisely, and the values are summarized in Table 1 together with their chemical compositions. The "*a*" parameter of LDHs correspond to the average cation−cation distance within the brucite-like layer and could be calculated as $a = 2 \times d(110)$. On the other hand, the "*c*" parameter is related to the thickness of the brucite-like layer and the interlayer distance and could be determined by averaging the d values of the (003) and (006) peaks using the formula: $c/3 = {}^1/_2\{d(003) + [2 \times d(006)]\}$.[20] It can be noticed from the table that the "*a*" parameter increases by about 0.018 Å for NiAl-LDH and about 0.029 Å for CoAl-LDH while the "*c*" parameter decreases by about 0.526 Å for NiAl-LDH and about 0.297 Å for CoAl-LDH when Sn^{4+} coexists in the M(II)Al-LDHs [M(II) = Ni or Co]. It should also be noted that the M(II):Al atomic ratio in each pair of the materials is kept constant (∼3.0) while adding the

(9) Velu, S.; Suzuki, K.; Okazaki, M.; Osaki, T.; Tomura, S.; Ohashi, F. *Chem. Mater.* **1999,** *11*, 2163.
(10) Kamath, P. V.; Therese, G. H. A. *J. Solid State Chem.* **1997**, *128*, 38.
(11) Xu, Z. P.; Zeng, H. C. *J. Mater. Chem.* **1998**, *8*, 2499.
(12) Severin, K. G.; Abdel-Fattah, T. M.; Pinnavaia, T. J. *Chem. Commun.* **1998**, 1471.
(13) Chaudhari, K.; Das, T. K.; Rajamohanan, P. R.; Lazar, K.; Sivasanker, S.; Chandwadkar, A. J. *J. Catal.* **1999**, *183*, 281.
(14) Gomez, R.; Sanchez, J.; Silva R.; Lopez, T. *React. Kinet. Catal. Lett.* **1996**, *59*, 247.
(15) Stork, S.; Maier, W. F.; Salrado, I. M. M.; Ferreria, J. M. F.; Guhl, D.; Souverijns, W.; Martens, J. A. *J. Catal.* **1997,** *172*, 414.
(16) FujiKawa, T.; Ribeiro, F. H.; Somorjai, G. A. *J. Catal.* **1998**, *178*, 58.
(17) Trimm, D. L. *Catal. Today* **1999**, 49, 3.
(18) Cullity, B. D. *Elements of X-ray diffraction*; Addition-Wesley: Reading, MA, 1959.
(19) Monti, D. A. M.; Baiker, A. *J. Catal.* **1983**, *83*, 323.
(20) Del Arco, M.; Malet, P.; Trujillano, R.; Rives, V. *Chem. Mater.* **1999**, *11*, 624.

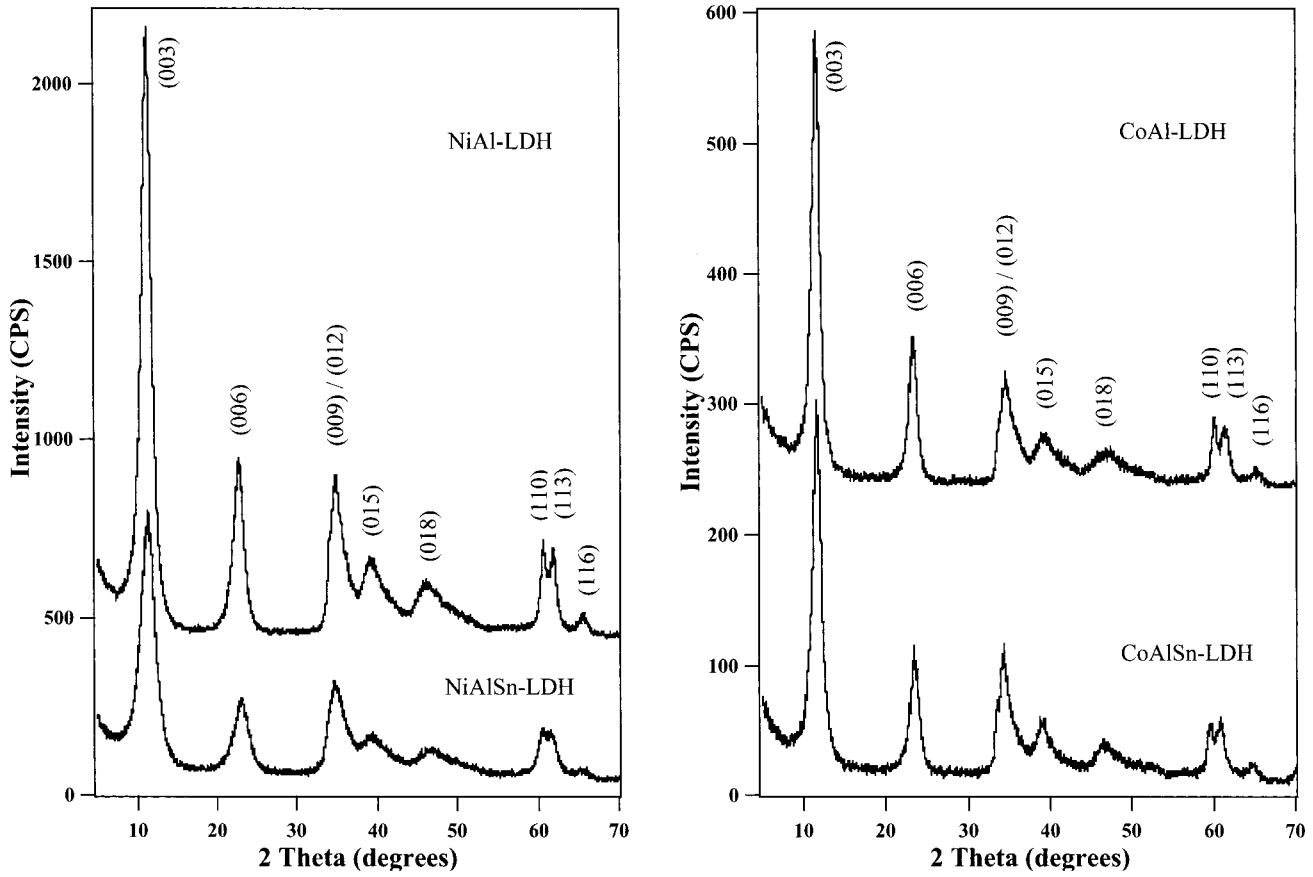

Figure 1. XRD patterns of NiAl-, NiAlSn-, CoAl-, and CoAlSn-LDHs recorded with a scan speed of 0.5° 2θ/min; step size: 0.01° 2θ.

Table 1. Chemical Composition and Lattice Parameters of M(II)Al- and M(II)AlSn-LDHs [M(II) = Ni or Co]

compound	M(II):Al:Sn atomic ratio[a]	M(II)/Al	M(II)/(Al + Sn)	lattice parameters (Å) *a*	lattice parameters (Å) *c*	fwhm[b] (2θ)	t^c (Å)	chemical formula[d]
NiAl-LDH	3:1.00:0.00	2.88	2.88	3.046	23.280	1.45	55	$Ni_{0.75}Al_{0.25}Sn_{0.00}(OH)_2(CO_3)_{0.13}\cdot 0.49H_2O$
NiAlSn-LDH	3:0.95:0.40	3.16	2.22	3.064	22.754	1.97	41	$Ni_{0.75}Al_{0.24}Sn_{0.10}(OH)_2(CO_3)_{0.31}\cdot 0.61H_2O$
CoAl-LDH	3:0.86:0.00	3.49	3.49	3.074	23.047	1.05	76	$Co_{0.75}Al_{0.22}Sn_{0.00}(OH)_2(CO_3)_{0.13}\cdot 0.33H_2O$
CoAlSn-LDH	3:0.93:0.36	3.23	2.33	3.103	22.750	1.18	68	$Co_{0.75}Al_{0.23}Sn_{0.10}(OH)_2(CO_3)_{0.28}\cdot 0.41H_2O$

[a] Determined by X-ray fluorescence spectroscopy. [b] Average values of Full width at half-maximum (fwhm) of (003) and (006) planes. [c] Crystallite size (*t*) calculated from (003) and (006) planes using Debye−Scherrer equation. [d] Chemical formulas derived from XRF and TG results assuming a M(II)/[M(III) + M(IV)] ratio of 3.0 for all compounds.

required amount of Sn salt during preparation. Hence, if Sn^{4+} had not been incorporated the lattice parameters of the Sn-containing LDHs and the non-Sn-containing LDHs would have been the same because of a similar M(II):Al atomic ratio. In contrast, the observed expansion in the "*a*" parameter clearly indicates that the Sn^{4+} isomorphously substitutes the Al^{3+} in their LDHs framework (ionic radii of Ni^{2+}, Co^{2+}, Al^{3+}, and Sn^{4+} in their octahedral coordination are 0.83, 0.89, 0.68, and 0.83 Å, respectively).[21] Although, a similar expansion in the "*c*" parameter would be expected, the observed contraction could be explained on the basis of an increase in attractive force between the brucite-like layer and the interlayer. This is because of an increase in charge density of the brucite-like layer since a tetravalent cation Sn^{4+} occupies the layer framework.[9]

It is also observed from the XRD patterns that the intensity or sharpness of all the diffraction peaks is reduced upon Sn incorporation. This is not surprising, as many researchers have observed a variation in crystallinity of LDHs when a cation (divalent or trivalent) is substituted by another isovalent cation having a similar ionic radius.[22−24] For example, a decrease in crystallinity of LDH is observed when a part of Mg^{2+} was substituted by Ni^{2+} in the synthesis of MgNiAl-LDH, a well-characterized system, despite the fact that the ionic radii of Mg^{2+} (0.86 Å) is very close to that of Ni^{2+} (0.83 Å).[22] A similar effect was also noticed in many other LDH systems.[23,24] Hence, in the present study, the decrease in crystallinity of LDHs upon Sn incorporation could be due to the isomorphous substitution of Sn, a tetravalent cation, for Al^{3+} in the brucite-like layer. As a measure of crystallinity of the LDH phase in the "*c*" axis direction, the full width at half-maximum (fwhm) value of (003) and (006) planes and the crystallite sizes calculated using Sherrer equation are also included in Table 1. It can be observed that the fwhm values are

(21) Huheey, J. E.; Keiter, E. A.; Keiter, R. L. *Inorganic Chemistry: Principles of Structure and Reactivity*, 4th ed.; Harper Collins College Publishers: New York, 1993.

(22) Tichit, D.; Medina, F.; Coq. B.; Dutartre, R. *Appl. Catal. A: Gen.* **1997**, *159*, 241.

(23) Kloprogge, J. T.; Frost, R. L. *Appl. Catal. A.* **1999**, *184*, 61.

(24) Ribet, S.; Tichit, D.; Coq, B.; Ducourant, B.; Morato, F. *J. Solid State Chem.* **1999**, *142*, 382.

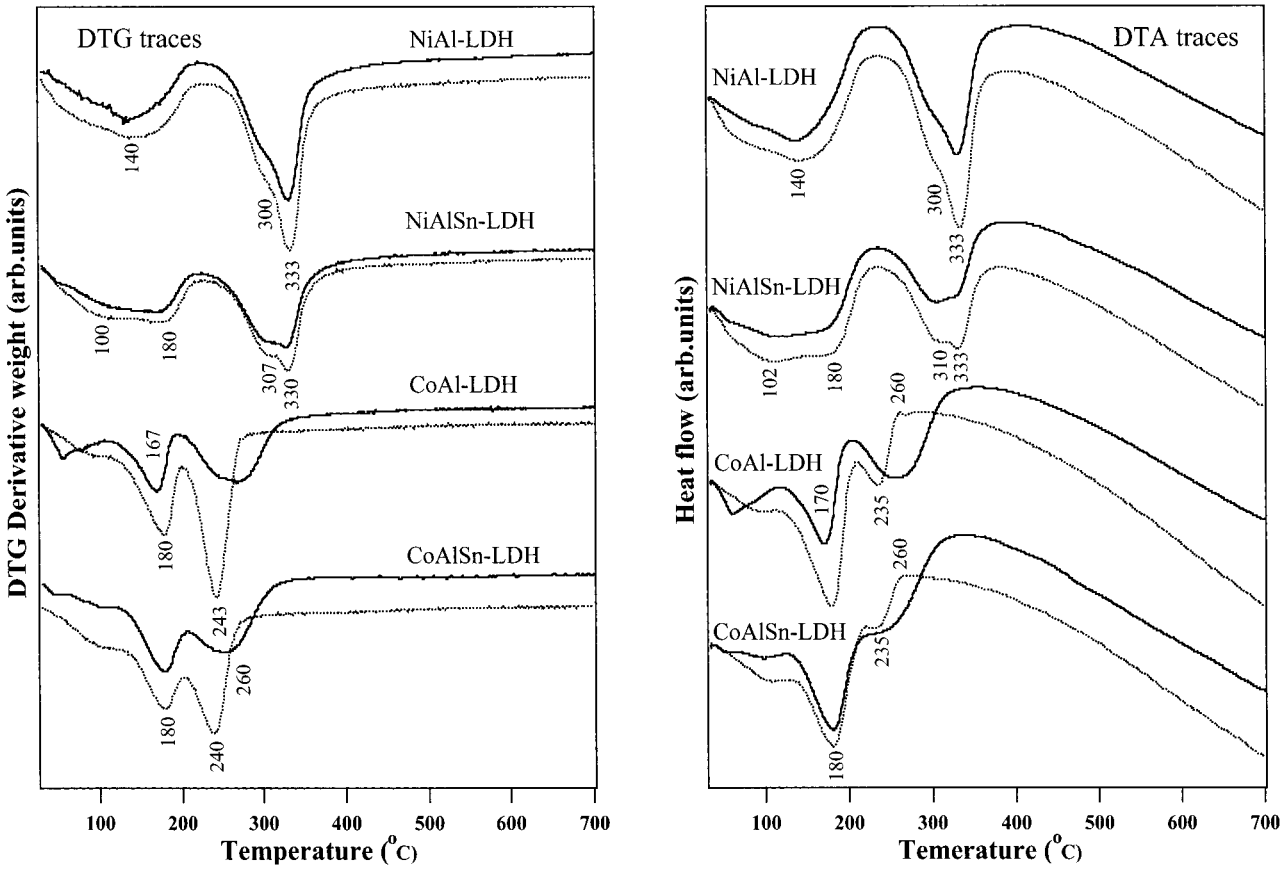

Figure 2. DTG and DTA traces of NiAl-, NiAlSn-, CoAl-, and CoAlSn-LDHs recorded in atmospheres of N_2 (solid line) and air (dotted line).

higher and the crystallite sizes are smaller for the Sn-incorporated LDHs compare to their non-Sn-containing analogues.

Thermogravimetry and Differential Thermal Analyses (TG/DTA). The thermal stability of M(II)Al-LDHs and their Sn-incorporated counterparts was examined by simultaneous TG/DTA experiments performed in both N_2 as well as in air atmospheres and the curves are shown in Figure 2. For the sake of clarity, the differential curves of TG (DTG) are presented. It is therefore convenient to compare the TG weight loss processes with those of the enthalpy changes occurring during the thermal transformations of LDHs. It is interesting to note that the shape and the endothermic transformation temperatures in DTA of NiAl- and NiAlSn-LDH recorded in both N_2 and air atmospheres are identical with those of the DTG traces, indicating that the endothermic transformations in DTA correspond to the weight loss process recorded in TG. Additional peaks were not found in the DTA of samples performed in N_2 atmosphere, confirming that phases other than LDH do not exist in these samples. The NiAl-LDH exhibits two major endothermic weight loss processes similar to that of MgAl-LDH.[9] The first weight loss process (T_1) in the temperature range 100−200 °C has been attributed to the loss of interlayer water and, the second weight loss process (T_2) occurring in the temperature range 200−400 °C has been ascribed to the loss of structural water and CO_2 from the interlayer because of the destruction of layered structure. It should also be noted that the T_1 peaks in both NiAl- and NiAlSn-LDH are very broad probably because of a heterogeneous distribution of water molecules in the interlayer of these materials. Furthermore, in NiAl-LDH, the T_2 peak shows a shoulder at ∼300° C while it appears as a doublet or two overlapped peaks in the NiAlSn-LDH. This result reveals that the T_2 is associated with some complex process such as the decomposition of CO_3^{2-} ion held with different strengths in the interlayer space and the destruction of M−OH bonds (Ni−OH, Al−OH/Sn−OH). A net weight loss of around 35−40% has been registered in these samples up to 450 °C.

The DTG patterns of CoAl- and CoAlSn-LDHs recorded in both N_2 and air atmospheres display two stages of weight loss processes similar to those observed in the Mg- and Ni-containing analogues. However, the peaks are relatively more intense and sharp, especially for those recorded in the air atmosphere. Furthermore, compare to the Ni-containing analogues the T_2 peaks are shifted toward low temperatures, indicating that the Co-containing LDHs are thermally less stable because of the presence of an oxidizable cation, Co^{2+}. In fact, the Co-containing LDHs offer corresponding spinel phases upon calcination above 200 °C (vide infra). The DTA curves of the samples recorded in air show a sharp single endothermic peak ∼180 °C, corresponding to the T_1 process recorded in DTG. The second endothermic peak corresponding to the T_2 process is very weak. Also, an exothermic very weak peak ∼260 °C is registered in both CoAl- and CoAlSn-LDHs. These results infer that the oxidation of Co^{2+} to Co^{3+}, presumably an exothermic process, takes place in the same temperature range as that of the endothermic decomposition of interlayer

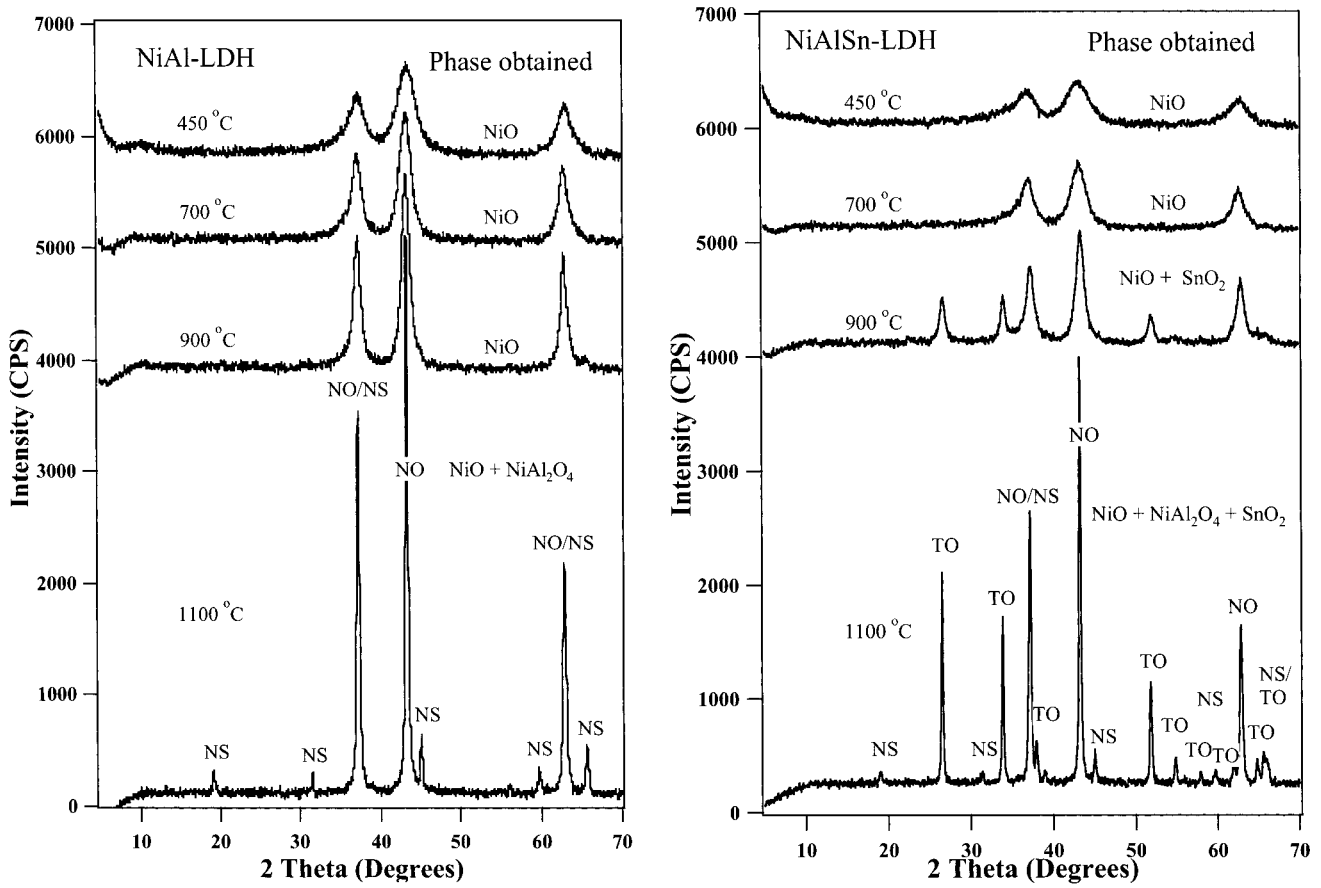

Figure 3. XRD patterns of NiAl- and NiAlSn-LDHs calcined at different temperatures for 5 h (scan speed, 2° 2θ/min; step size, 0.02° 2θ). (NO) = NiO, (NS) = $NiAl_2O_4$, (TO) = SnO_2.

Table 2. Structural Properties of NiAl- and NiAlSn-LDHs Calcined at Different Temperatures

	NiAl-LDH		NiAlSn-LDH			literature value	
calcination temperature (°C)	phase obtained	lattice parameter (Å)	phase obtained	lattice parameter (Å)	Δ^a	phase	lattice parameter (Å)
450	NiO	$a = 4.166$	NiO	$a = 4.182$	0.016	NiO	$a = 4.177$
700	NiO	$a = 4.170$	NiO	$a = 4.180$	0.010		
900	NiO	$a = 4.175$	NiO	$a = 4.176$	0.001		
	+		+			$NiAl_2O_4$	$a = 8.048$
	$NiAl_2O_4$	ND[c]	$NiAl_2O_4$	ND[c]	–		
			+			SnO_2	$a = 4.738$
			SnO_2	$a = 4.711$	0.027[b]		$c = 3.187$
				$c = 3.188$	0.001[b]		
1100	NiO	$a = 4.178$	NiO	$a = 4.179$	0.001		
	+		+				
	$NiAl_2O_4$	$a = 8.043$	$NiAl_2O_4$	$a = 8.041$	0.002		
			+				
			SnO_2	$a = 4.740$	0.002[b]		
				$c = 3.184$	0.003[b]		

[a] Difference in lattice parameters between NiAl-LDH and NiAlSn-LDH calcined at indicated temperatures for 5h. [b] Difference in lattice parameters between SnO_2 derived in situ and the literature value. [c] ND = Not determined.

CO_3^{2-} ion and the hydroxyl layer in the T_2 region. As a result, the endothermic effects are completely canceled by the exothermic effects and hence they appear as very weak peaks (see Figure 2, DTA traces). Similar results were also observed in an earlier study on the CoAl-LDH system.[25]

XRD of Calcined Samples. Figure 3 shows the XRD patterns of NiAl- and NiAlSn-LDHs calcined at various temperatures while the lattice parameters of their thermally transformed products are collected in Table 2. Calcination of NiAl-LDH at 450 °C offers a rock salt-type NiO phase. The lattice parameter of the resulting NiO phase is slightly less than that of the literature value, indicating the formation of an Al-doped NiO solid solution represented by the formula $NiAl_{2\delta}O_{1+3\delta}$.[26] Earlier studies[27] have demonstrated that the Al-doped NiO crystallites revert back to the original layered structure (memory effect) when it is brought in to

(25) Ulibarri, M. A.; Fernandez, J. M.; Labajos, F. M.; Rives, V. *Chem. Mater.* **1991**, *3*, 626.

(26) Kannan, S.; Narayanan, A.; Swamy, C. S. *J. Mater. Sci.* **1996**, *31*, 2353.

(27) Courty, Ph.; Marcilly, C. In *Preparation of catalysts III*; Poncelet, G., Grange, P., Jacobs, P. A., Eds.; Elsevier: Amsterdam, 1983; pp 485–517.

contact with an aqueous solution; however, under severe hydrothermal conditions. The crystallinity of the solid solution increases upon increasing the calcination temperature to 700 and 900 °C. Recently, a decoration model has been proposed for the NiAl-LDH calcined in the temperature range 400−800 °C, which suggested that the NiO crystallites are decorated by spinel-type phases.[28,29] The lattice parameter of the NiO solid solution in the present study increases progressively and attains a value similar to that of the pure NiO at 900 °C, indicating that the NiO distortion becomes negligible at higher calcination temperatures. Calcination at 1100 °C resulted in the disproportionation of the material to form discrete particles of NiO and $NiAl_2O_4$ spinel phases.

The NiAlSn-LDH also offers a poorly crystallized NiO-like phase at 450 °C (see Figure 3). However, the lattice parameter of the resulting NiO phase is higher compare to the non-Sn-containing counterpart and it is similar compare to the literature value (see Table 2). These results indicate that some amounts of Sn^{4+} would have been incorporated besides Al^{3+} in the NiO lattice, giving rise to a solid solution similar to that obtained from the NiAl-LDH. Furthermore, as noticed in the uncalcined samples, the crystallinity of the calcined materials at all the temperatures is less compare to the non-Sn-containing materials because of the isomorphous presence of Sn^{4+} in the calcined samples. The crystallinity of NiO phase increases with further increases in calcination temperature to 700 and 900 °C, indicating a progressive improvement in the crystallinity of the solid solution. However, for the sample calcined at 900 °C, besides NiO, the appearance of another Sn-containing phase is evident. It should be mentioned that Sn crystallized out as Mg_2SnO_4 spinel from a similar Mg-containing analogue in the same calcination temperature.[9] However, the existence of a similar Ni_2SnO_4 phase is not known in the literature, while only the $NiSnO_3$ phase has been reported (JCPDS file no. 28-711). Interestingly, the observed XRD pattern fits well with that of cassiterite (SnO_2; JCPDS file no. 41-1445) rather than the $NiSnO_3$ spinel. The appearance of the SnO_2 phase along with NiO and $NiAl_2O_4$ phases is clearly observed in the sample calcined at 1100 °C. The lattice parameters of the SnO_2 phase derived in situ from these materials was calculated with tetragonal crystalline phase using the relation:[18] $\sin^2\theta = A(h^2 + k^2) + Cl^2$, where, $A = \lambda^2/4a^2$ and $C = \lambda^2/4c^2$. Thus, the $d(110)$ and $d(200)$ planes of resulting SnO_2 phase were used for the calculation of "*a*" parameter, while the "*c*" parameter was calculated from the $d(101)$ and $d(211)$ planes. The calculated lattice parameters "*a*" and "*c*" are in agreement with those of the literature data (Table 2). The coincidence of lattice parameters of SnO_2 with those of the literature data implies that Ni^{2+} and/or Al^{3+} cations are not present in the SnO_2 lattice derived from NiAlSn-LDH.

Unlike Ni-containing analogues, the product obtained during thermal decomposition of CoAl-LDH is rather complex. Since, the thermal analysis of the Co-containing analogues (Figure 2) showed that the material decomposes relative to lower temperatures of about 250 °C, the XRD pattern was recorded for sample calcined at 300 °C as well. Figure 4 depicts the XRD patterns of CoAl-LDH calcined at different temperatures. The rock salt-type CoO is not observed even at 300 °C, instead, the XRD pattern corresponded to a nonstoichiometric spinel phase similar to Co_3O_4, $CoAl_2O_4$, or Co_2AlO_4. The formation of spinel phases even at low temperatures is not surprising as CoO is thermodynamically less stable compared to other spinels in the intermediate temperatures (For example, CoO; $\Delta G°_f = -214$ kJ mol Co^{-1}, Co_3O_4; $\Delta G°_f = -258$ kJ mol Co^{-1}).[30] However, the XRD pattern and the lattice constant of the Co_3O_4 spinel are comparable with those of $CoAl_2O_4$ or Co_2AlO_4 ("*a*" parameters of Co_3O_4, $CoAl_2O_4$, and Co_2AlO_4 are 8.084; JCPDS file no. 42-1467, 8.103; JCPDS file no. 10-458, and 8.086 Å; JCPDS file no. 38-814, respectively; see Table 3). Best fit was observed for $CoAl_2O_4$ and Co_3O_4. In fact in an earlier study[25] on the similar CoAl-LDH, it has been reported that Co_3O_4 was the only crystalline phase formed in the calcination temperature 238−320 °C, while a mixture of Co_3O_4, $CoAl_2O_4$ and Co_2AlO_4 phases could be formed at higher calcination temperatures. Our XRD data, however, reveals that Co_3O_4 may not be a single crystalline phase at this temperature and it is possible that a mixture of Co_3O_4 and $CoAl_2O_4$ or a solid solution of these two spinels would have been formed. This argument will be further substantiated by the TPR results in the next section. Taking into account the initial composition of Co and Al (atomic ratio of 3:0.86) in the parent LDH precursor, and also the fact that only the spinel phase is present, it is reasonable to assume that the spinel phase would correspond to a nonstoichiometric material whose composition can be either $Co^{2+}Al_{2-x}Co^{3+}{}_xO_4$ or $Co^{2+}Co^{3+}{}_{2-x}Al_xO_4$. The formula indicates that either Co^{3+} can substitute for Al^{3+} in the $CoAl_2O_4$ spinel or the Al^{3+} can substitute for Co^{3+} in the Co_3O_4 spinel. It should be remembered that in spinels, the trivalent cations occupy the octahedral sites and that Co^{3+} in spinels occurs in the low-spin configuration. Hence, if Co^{3+} substitutes for Al^{3+}, there should be a small decrease in the lattice parameter of the $CoAl_2O_4$ phase. Alternatively, if Al^{3+} substitutes for Co^{3+} in Co_3O_4 then the lattice parameter of the resulting spinel would be slightly higher than that of the Co_3O_4 spinel. However, the lattice parameter variation depends on extent of substitution. It can be noted from the Table 3 that the lattice constant of the resulting Co-spinel at all the calcination temperatures is considerably less (within the experimental errors) than that of the $CoAl_2O_4$ and more or less similar compared to that of Co_3O_4 spinel. These results indicate that Co^{3+} possibly substitutes for Al^{3+} in $CoAl_2O_4$ to form a nonstoichiometric spinel of $Co^{2+}Al_{2-x}Co^{3+}{}_xO_4$. The value of *x* would depend on the calcination temperature and hence a variation in the lattice parameter is observed. Since, the sample calcined at 1100 °C is highly crystalline, the value of $x \approx 1.326$ can be calculated from the initial composition of Co and Al. Our assignment is in agreement with a recent report[30] on the similar CoFe-LDH, which upon calcination around 400 °C yielded a nonstoichio-

(28) Rebours, B.; Caillerie, J.; Clause, O. *J. Am. Chem. Soc.* **1994**, *116*, 1707.

(29) Fornasari, G.; Gazzano, M.; Matteuzzi, D.; Trifiro, F.; Vaccari, A. *Appl. Clay Sci.* **1995**, *10*, 69.

(30) Del Arco, M.; Trujillano, R.; Rives, V. *J. Mater. Chem.* **1998**, *8*, 761.

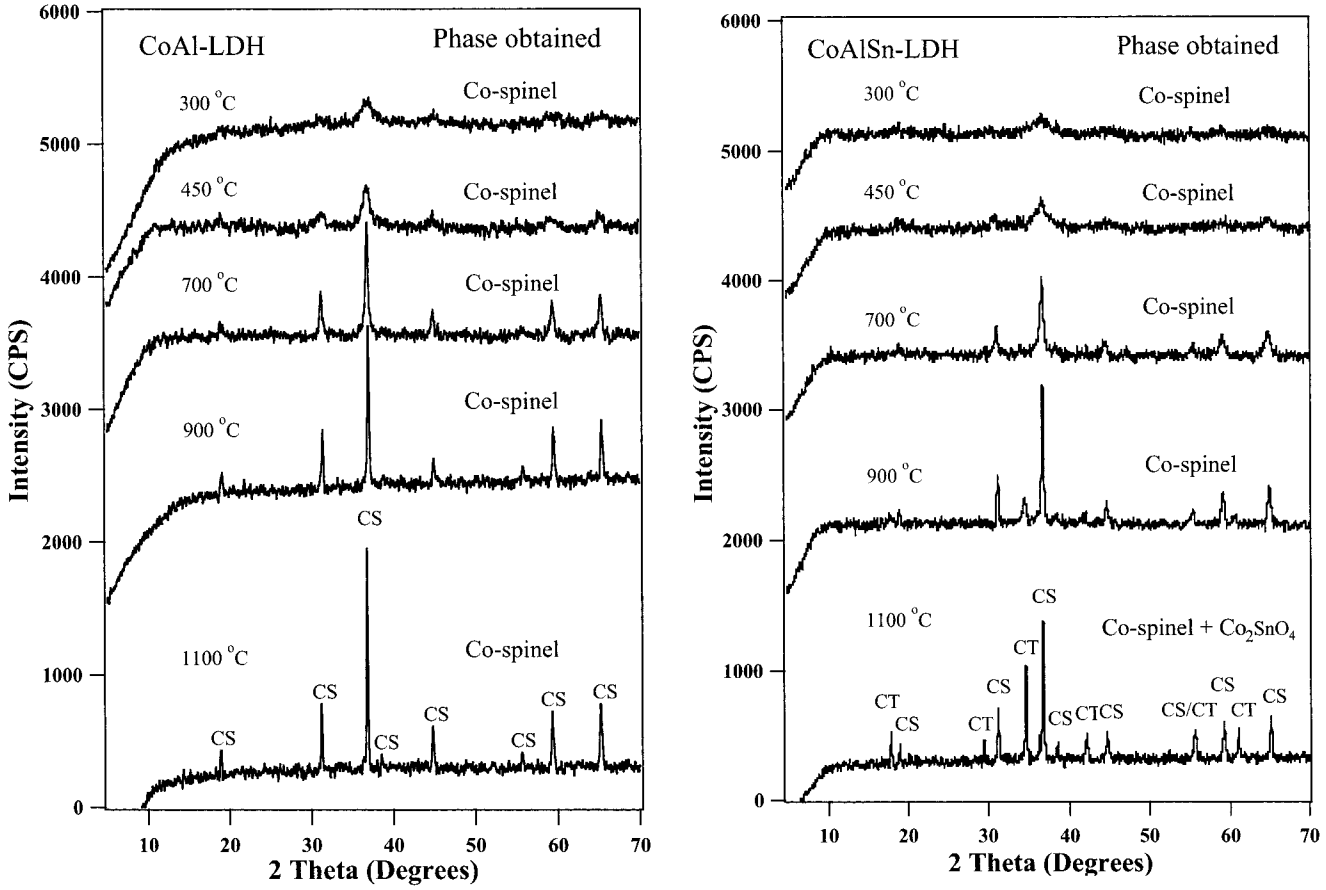

Figure 4. XRD patterns of CoAl- and CoAlSn-LDHs calcined at different temperatures for 5 h (scan speed, 2° 2θ/min; step size, 0.02° 2θ). (CS) = nonstoichiometric Co spinel, (CT) = Co_2SnO_4 inverse spinel.

Table 3. Structural Properties of CoAl- and CoAlSn-LDHs Calcined at Different Temperatures

	CoAl-LDH		CoAlSn-LDH			literature value	
calcination temperature (°C)	phase obtained	lattice parameter (Å)	phase obtained	lattice parameter (Å)	Δ^a	phase	lattice parameter (Å)
300	Co-spinel	$a = 8.083$	Co-spinel	$a = 8.103$	0.020	Co_3O_4	$a = 8.084$
450	Co-spinel	$a = 8.076$	Co-spinel	$a = 8.096$	0.020	$CoAl_2O_4$	$a = 8.103$
700	Co-spinel	$a = 8.070$	Co-spinel	$a = 8.104$	0.034	Co_2AlO_4	$a = 8.086$
900	Co-spinel	$a = 8.071$	Co-spinel + Co_2SnO_4	$a = 8.106$ ND[c]	0.035 –	Co_2SnO_4	$a = 8.638$
1100	Co-spinel	$a = 8.088$	Co-spinel + Co_2SnO_4	$a = 8.099$ $a = 8.578$	0.011 0.060[b]		

[a] Difference in lattice parameters between CoAl-LDH and CoAlSn-LDH calcined at the indicated temperatures for 5h. [b] Difference in lattice parameter between Co_2SnO_4 inverse spinel derived in situ and the literature value. [c] ND = Not determined.

metric spinel having a composition $Co^{2+}Fe^{3+}_{2-x}Co^{3+}_xO_4$.

The Sn-incorporated analogue also exhibits similar XRD patterns in the temperature range 300−700 °C. However, the lattice parameters of the resulting Co-spinel phase are higher than that derived from the non-Sn-containing analogues, indicating that some amounts of Al^{3+} or Co^{3+} are isomorphously substituted by Sn^{4+} in the nonstoichiometric spinel. The resulting material can thus be represented as $Co^{2+}Al_{2-(x+y)}Co^{3+}_xSn^{4+}_yO_{4+y/2}$ or $Co^{2+}Co^{3+}_{2-(x+y)}Al_xSn^{4+}_yO_{4+y/2}$. A further calcination of CoAlSn-LDH at 900 °C develops additional XRD lines, whose intensity increases with further increasing calcination temperature to 1100 °C. The XRD pattern of the additional phase corresponds to that of Co_2SnO_4 inverse spinel, which is similar to that noticed in the Mg-containing analogue.[9] The lattice constant of Co_2SnO_4 (8.578 Å) is lower compared to that of the literature value (8.638 Å), indicating that Al^{3+} isomorphously substitutes a part of Sn^{4+} in the Co_2SnO_4 spinel. No XRD peaks corresponding to the SnO_2 phase could be detected in these samples, indicating that the decomposition of CoAlSn-LDH follows a different pathway compared to that of NiAlSn-LDH.

TPR Study. LDHs containing transition metal ions in the layer are being used as catalyst precursors for many industrially important reactions. For example, the Al-doped NiO systems are employed as catalyst for the steam re-forming of methane to synthesis gas and, for this reason these catalytic systems received much attention in the recent years.[3,31] Similarly, catalysts derived from CoAl-LDHs have recently proven to be the most efficient for the decomposition of N_2O, the green house gas, into N_2 and O_2.[32,33] Hence, the study of redox properties of the LDHs and their thermally transformed

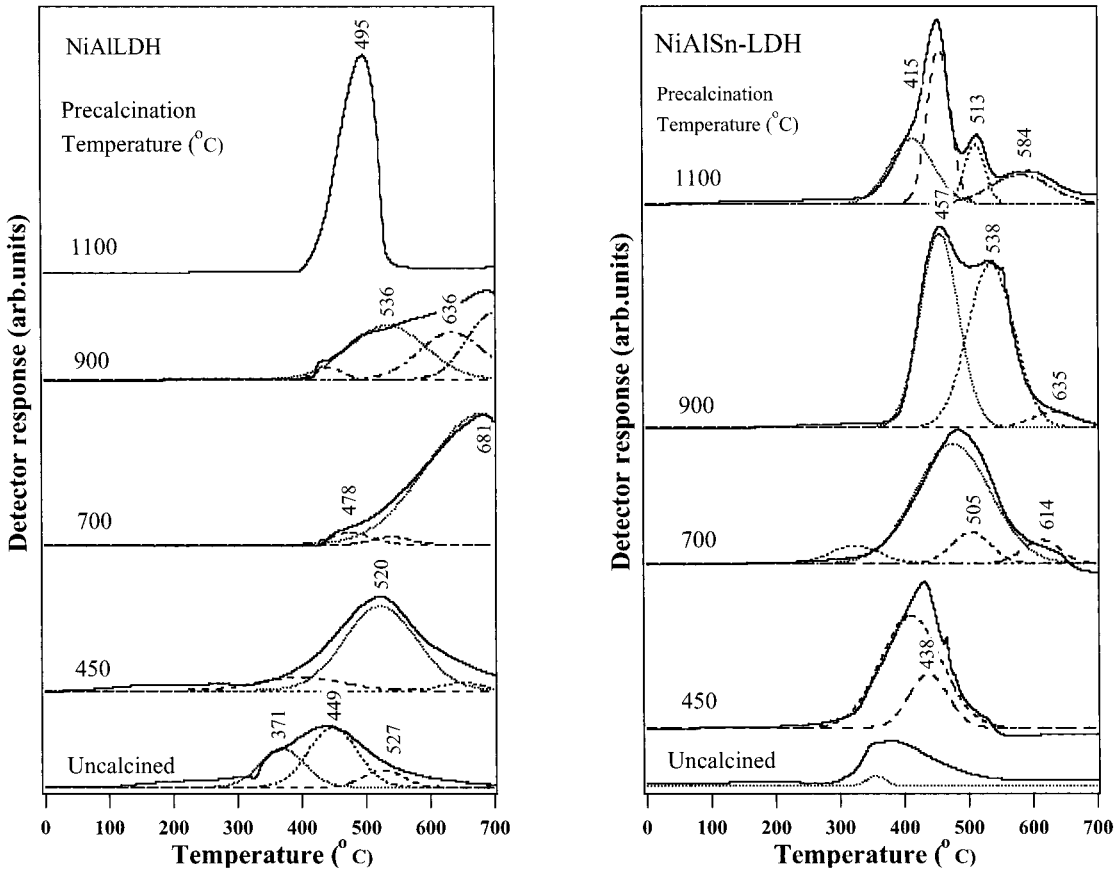

Figure 5. TPR profiles of NiAl- and NiAlSn-LDHs calcined at different temperatures for 5 h. Solid lines are experimental curves, and dotted lines are deconvoluted curves.

products is very useful to understanding the nature of Ni or Co species present at each calcination temperatures. We investigated here the effect of Sn incorporation on the reducibility of NiAl- and CoAl-LDHs and their thermally derived products by TPR experiments. The TPR profiles are shown in Figures 5−7 while the quantitative data of the samples extracted by deconvolution of original TPR profiles are summarized in Tables 4 and 5.

The TPR patterns of samples derived from NiAl-LDH are compared with those of NiAlSn-LDH in Figure 5. The uncalcined sample of NiAl-LDH exhibits a peak (54.9%) at 449 °C together with shoulders at 371 and 527 °C. From the value of H_2 consumption, the ratio of H_2(mol)/amount of Ni (mol) in the NiAl-LDH was calculated to be 1.12. This means, the H_2 consumption corresponds to the reduction of $Ni^{2+} \rightarrow Ni^0$ in the LDH. In a recent TPR study[34] the reduction of takovite (NiAl-LDH with Ni:Al atomic ratio = 3) was recorded at around 400 °C. For samples calcined between 450 and 900 °C, reduction is being observed at all temperatures from 400 to 700 °C. The temperature required for maximum rate of H_2 consumption increases dramatically upon increasing the calcination temperature up

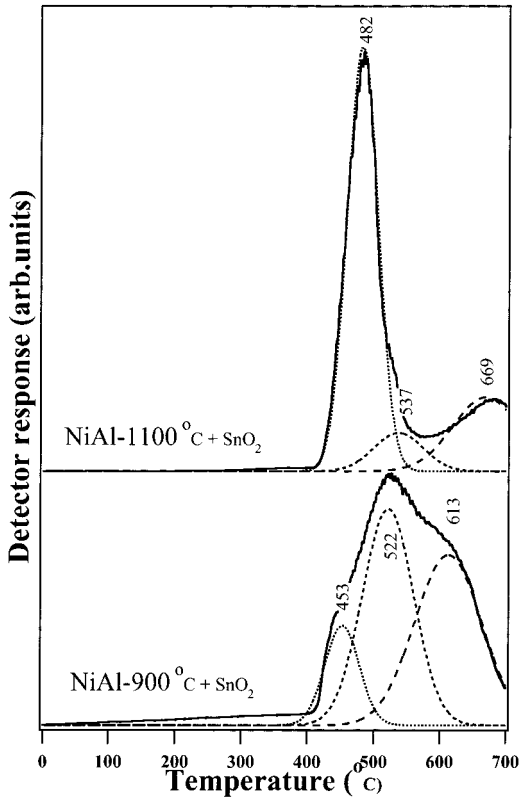

Figure 6. TPR profiles of physical mixture of NiAl-LDH calcined at 900 °C + 20 wt % of SnO_2, subsequently calcined at 900 °C/5 h and NiAl-LDH calcined at 1100 °C +20 wt % of SnO_2, subsequently calcined at 1100 °C/5h. Solid lines are experimental curves, and dotted lines are deconvoluted curves.

(31) Basile, F.; Basini, L.; Amore, M. D.; Fornasari, G.; Guarinoni, A.; Matteuzzi, D.; Piero, G. D.; Trifiro F.; Vaccari, A. *J. Catal.* **1998,** *173*, 247.
(32) Kannan, S.; Swamy, C. S. *Appl. Catal. B* **1994**, *3*, 109.
(33) Armor, J. N.; Braymer, T. A.; Farris, T. S.; Li, Y.; Petrocelli, F. P.; Weist, E. L.; Kannan, S.; Swamy, C. S. *Appl. Catal. B* **1996**, *7*, 397.
(34) Rives, V.; Ulibarri, M. A.; Montero, A. *Appl. Clay Sci.* **1995**, *10*, 83.

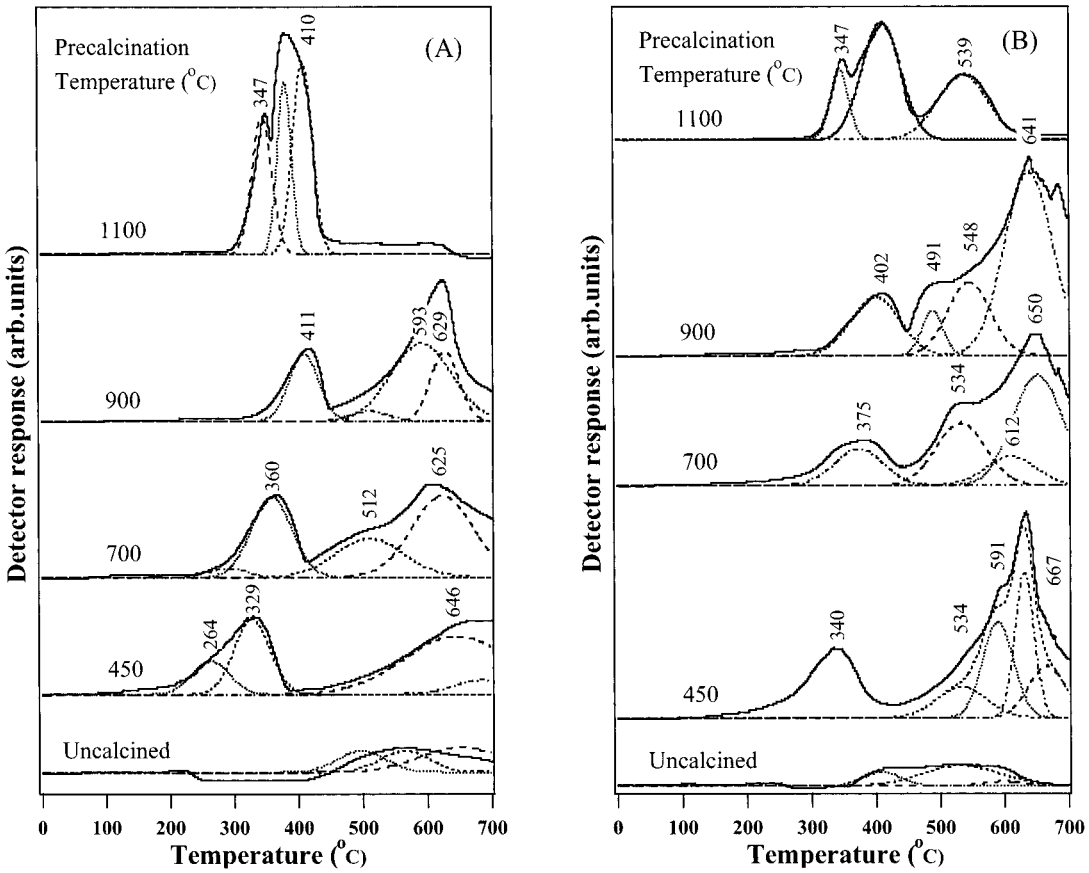

Figure 7. TPR profiles of (A) CoAl-LDH and (B) CoAlSn-LDH, calcined at different temperatures for 5 h. Solid lines are experimental curves, and dotted lines are deconvoluted curves.

Table 4. Quantitative TPR Data of NiAl- and NiAlSn-LDHs Calcined at Different Temperatures

	peak positions (°C) and quantity (%) of each species determined by the deconvolution of TPR peaks[a]									
	NiAl-LDH					NiAlSn-LDH				
precalcination temperature (°C)	peak 1	peak 2	peak 3	peak 4	mol H_2/mol Ni	peak 1	peak 2	peak 3	peak 4	mol H_2/mol Ni + Sn
uncalcined	371 (32.3)	449 (54.9)	527 (12.8)	–	1.12	–	–	–	–	0.60
450	399 (14.4)	524 (81.4)	651 (4.2)	–	0.69	278 (6.3)	411 (68.7)	438 (21.0)	521 (4.0)	0.93
700	478 (3.4)	541 (94.5)	681 (2.1)	–	1.03	477 (81.4)	505 (10.8)	614 (7.8)	–	1.21
900	446 (3.0)	536 (38.0)	636 (27.9)	699 (31.1)	1.03	457 (47.4)	538 (48.2)	635 (4.4)	–	2.40
1100	500 (100)	–	–	–	1.42	415 (30.5)	457 (38.3)	513 (12.8)	584 (18.4)	1.58

[a] Values in the parentheses are percentage of each species extracted from the deconvolution of the original TPR profiles.

to 700 °C and then decreases on further calcination (see Figure 5 and Table 4). Moreover, the peaks did not recover the baseline, indicating that the reduction of Ni^{2+} in the NiO and/or $NiAl_2O_4$ spinel is incomplete. The observed decrease in reducibility of samples calcined up to 700 °C could be due to a lower accessibility of samples to the reducing gas possibly because of the presence of a nonstoichiometric spinel type phase decorating the NiO particles. A three-phase model containing (i) an Al-doped NiO crystallite, (ii) a Ni-doped alumina, and (iii) an aluminate spinel-type phase at the NiO−alumina interface has been proposed to be formed during the calcination of NiAl-LDHs[28,29]. So, the Ni^{2+} in these calcined samples should be present at least in three different chemical environments. Each Ni^{2+} species would then become reduced at different temperatures as evidenced from the TPR profiles, which shows three or four peaks on deconvolution. In contrast, for the sample calcined at 1100 °C, the TPR shows a sharp signal centering at 495 °C. This is because, at higher calcination temperatures a structural rearrangement takes place with formation of stoichiometric aluminate and oxide phase as supported by the XRD data which indicated the crystallization of well-defined phases of NiO and $NiAl_2O_4$ spinel (see Figure 3 and Table 2). Hence, the sharp and intense TPR peak for sample calcined at 1100 °C can be ascribed to the reduction of Ni^{2+} in these well-defined and highly crystalline NiO/$NiAl_2O_4$ phases.

The Sn-incorporated counterpart also shows similar TPR profiles. In all these samples, the reduction seems to be completed before 700 °C. The maximum rate of

Table 5. Quantitative TPR Data of CoAl- and CoAlSn-LDHs Calcined at Different Temperatures

	peak positions (°C) and quantity (%) of each species determined by the deconvolution of TPR peaks[a]									
	NiAl-LDH					NiAlSn-LDH				
precalcination temperature (°C)	peak 1	peak 2	peak 3	peak 4	mol H_2/mol Co	peak 1	peak 2	peak 3	peak 4	mol H_2/mol Co + Sn
uncalcined	498 (24.4)	565 (25.0)	653 (50.6)	–	0.43	409 (20.5)	461 (10.0)	533 (61.4)	599 (8.1)	0.62
450	264 (11.2)	329 (25.0)	646 (56.4)	687 (7.4)	1.10	340 (24.4)	534 (12.6)	591 (24.4)	632[b] (22.9)	1.53
700	293 (2.9)	360 (29.0)	512 (23.3)	625 (44.8)	1.33	375 (14.9)	534 (26.1)	612 (12.2)	654 (46.8)	1.61
900	411 (22.0)	511 (4.0)	593 (52.3)	629 (21.7)	1.46	402 (18.0)	491 (6.0)	548 (19.8)	641 (56.2)	2.02
1100	347 (30.3)	382 (27.4)	410 (42.3)	–	1.11	347 (13.8)	411 (50.5)	539 (35.6)	–	1.64
CoO (reference)	420				0.94					
Co_3O_4 (reference)	400				1.44					
$CoAl_2O_4$ (reference)[c]	392 (13.6)	603 (86.4)			1.10					
SnO_2 (reference)	690				1.93[d]					

[a] Values in the parentheses are percentage of each species extracted from the deconvolution of the original TPR profiles. [b] A fifth peak appeared at 667 °C with a contribution of 15.7%. [c] Prepared by the coprecipitation of $Co(NO_3)_2$ and $Al(NO_3)_3$ using NH_4OH solution followed by calcination at 500 °C. [d] Moles of H_2/moles of Sn.

H_2 consumption at each calcination temperatures is shifted toward a low temperature compared to their non-Sn-containing samples implying that the presence of Sn in the NiAl-LDH enhances the reducibility of Ni^{2+} species. It should be recalled that the formation of a separate SnO_2 phase was detected from the XRD of samples calcined around 900 °C. It is known that the SnO_2 exhibits redox properties and acts as a promoter in mixed oxide systems such as MoO_3/SnO_2, TiO_2/SnO_2 etc.[15,35] The SnO_2 in V_2O_5/SnO_2 catalytic system is known to facilitate the easier removal of terminal oxygen of V═O surface species thereby improving the catalytic performance in the ammoxidation reactions.[36] In view of this it is reasonable to state that the enhancement in the reducibility of Ni^{2+} species in the present study is due to the promoting action of SnO_2 in NiO crystallites. It should also be noted that under our experimental conditions, the pure SnO_2 reference sample became reduced in a single step with a peak centering at 690 °C (see Table 5). However, no other reduction peak was monitored above 700 °C when the TPR of some of these samples was extended up to 800 °C. This means, the reduction of Sn^{4+} is completed before 700 °C in the samples derived from NiAlSn-LDH. A careful comparison of the TPR data of samples derived from NiAl-LDH, NiAlSn-LDH and SnO_2 reference revealed that the peaks observed above 600 °C in Figure 5 (NiAlSn-LDH) are due to the reduction of Sn^{4+} to Sn^0. On the other hand, peaks recorded below 600 °C should correspond to the reduction of Ni^{2+} in $NiO/NiAl_2O_4$ in these samples. So, our results indicate that the reducibility of both Ni^{2+} as well as Sn^{4+} are enhanced in these samples, especially for those calcined above 700 °C, where XRD showed a mixture of $NiO/NiAl_2O_4$ and SnO_2 phases.

To further investigate if the SnO_2 in these samples is existing simply as a mixture or it has any interaction with $NiO/NiAl_2O_4$ phases, the TPR of two physical mixtures are also performed. Figure 6 shows the TPR profiles of physical mixtures of NiAl-LDH calcined at 900 °C or 1100 °C + 20 wt % of SnO_2. Both the mixtures were subsequently calcined at 900 and 1100 °C, respectively, before performing the TPR experiments so that the material in the physical mixture would be similar to that of the in situ derived material. In fact, the XRD data of the physical mixture prepared in the present study was similar to that of the in situ derived materials (XRD pattern not shown). If the intrinsic nature of the SnO_2 in the samples derived from NiAlSn-LDH is same as that of the physical mixtures, then one would expect similar TPR patterns and the reduction temperatures for Ni^{2+} and Sn^{4+} species. In contrast, differences in both the TPR patterns and the reduction temperatures are noticed between the physical mixtures and the in situ derived materials. For example, the physical mixture of NiAl-LDH calcined at 900 °C + SnO_2 exhibits a broad peak which can be resolved by deconvolution into three peaks, centering at 453, 522, and 613 °C, respectively. However, the in situ derived material exhibits a strong doublet, one centering at 457 °C, while the other at 538 °C together with a small shoulder around 635 °C. Similarly, the physical mixture of NiAl-LDH calcined at 1100 °C + SnO_2 shows an intense peak at 482 °C with a shoulder at 537 °C together with a broad peak around 669 °C. On the other hand, the in situ derived counterpart exhibits four peaks, which are centered at 415, 457, 513, and 584 °C, respectively. Furthermore, unlike in the in situ derived materials, the TPR profiles in the physical mixtures are not recovered at the baseline, indicating that the reduction of Sn is incomplete in these samples. These results clearly demonstrate that the intrinsic nature of Ni^{2+} and Sn^{4+} species in the in situ derived materials differ from that of the physical mixtures. The observed difference in the TPR data between the physical mixtures and the in situ derived materials could be attributed to an interaction existing between the Ni containg phase and the Sn-containing phase in the later samples although the XRD showed the presence of a separate SnO_2 phase along with NiO and $NiAl_2O_4$ phases. Such an interaction would be responsible for the observed increase in the

(35) Skolmeistere, R.; Leitis, L.; Shymanska, M.; Stochi, J. *Catal. Today* **1993**, *17*, 79.
(36) Lakshmi, J. L.; Alyea, E. C. *Catal. Lett.* **1999**, *59*, 73.

reducibility of both $Ni^{2+} \rightarrow Ni^0$ as well as $Sn^{4+} \rightarrow Sn^0$ if they were present together in the coprecipitated samples.

Figure 7 shows the TPR profiles of materials derived from CoAl- and CoAlSn-LDHs. The uncalcined samples of CoAl-LDH exhibits a broad peak above 450 °C. The ratio, H_2 (mol)/Co (mol) of 0.43 (see Table 5) is very low probably because of the incomplete reduction of Co species as the TPR profile did not recover at the baseline. For the sample calcined between 450 and 900 °C, three main reduction regions are distinguished. They are region I, in the temperature range 250−450 °C, region II between 450 and 550 °C, and region III above 550 °C. Deconvolution of original TPR curves exhibited four to five peaks, indicating the existence of several reducible species in these samples. Similar results were also noticed in MgCoAl-LDH systems[24] and in various supported cobalt catalysts. [37−39]

Region I (TPR Peak between 250 and 450 °C). The first and, relatively, a sharp peak in all the samples calcined above 300 °C appears in this region. It should be noted that reference samples of both CoO and Co_3O_4 are also reduced in the same region while $CoAl_2O_4$ prepared in our present study exhibited a broad peak centering at about 600 °C (see Table 5). The presence of CoO in the samples derived from CoAl-LDH is unlikely, and XRD of the samples showed the existence of a nonstoichiometric spinel with a composition either $Co^{2+}Co^{3+}_{2-x}Al_xO_4$ or $Co^{2+}Al_{2-x}Co^{3+}_xO_4$. They can also be considered as a mixture of Co_3O_4 and $CoAl_2O_4$ because the Co species in the above nonstoichiometric spinels will have chemical environments similar to both Co_3O_4 and $CoAl_2O_4$. It can be seen clearly from the TPR profiles of CoAl-LDH calcined at 450 °C which exhibits two distinct peaks in this region on deconvolution; one centering at 264 °C with a concentration of 11.2% and the other at 329 °C with a contribution of about 25%. These peaks are unambiguously attributed to the reduction of Co_3O_4, which generally occurs in two steps ($Co_3O_4 \rightarrow CoO \rightarrow Co$).[38] So, comparing the TPR results with those of the reference samples of CoO, Co_3O_4, and $CoAl_2O_4$, it is reasonable to state that the reduction in this region corresponds to the reduction of $Co^{2+}-Co^{3+}$ species in the nonstoichiometric spinel, having chemical environments similar to that of the Co_3O_4 spinel. On further calcination, the concentration of $Co^{2+}-Co^{3+}$ species reduced in this region decreases with consequent increase in the concentration of Co species that can be reduced in regions II and III. Additionally, the temperature for maximum rate of H_2 consumption for the peak in region I increases (see Table 5).

Region III (TPR Peaks above 550 °C). All the samples calcined in the temperature range 300−900 °C as well as the uncalcined sample exhibited TPR peaks above 550 °C. The reduction of $CoAl_2O_4$ prepared in the present study also exhibits a broad peak in this region. It should be noted that in the CoAl-LDH structure, Al^{3+} occupies the octahedra of the brucite-like $Co(OH)_2$ layer. Although, the LDH structure collapses before being reduced in TPR, the Co^{2+} ions are certainly surrounded by Al^{3+} ions. Hence, the reduction in this region can be attributed to the reduction of $Co^{2+}-Al^{3+}$ species, wherein the Co^{2+} ions have a large number of O−Al ligands. The resulting species behave chemically like $CoAl_2O_4$ spinel. This assignment is in line with the chemical formula of the nonstoichiometric spinels suggested for these samples. As mentioned previously, the Co_3O_4-like species present in the nonstoichiometric spinel are reduced in region I while the $CoAl_2O_4$-like species are reduced in region III. Deconvolution of the original TPR curves show at least two peaks in this region, indicating the existence of at least two different $Co^{2+}-Al^{3+}$ species. It has been suggested that for crystalline as well as for surface species, the number of Al^{3+} ions in the surrounding of the Co ion determines the reduction temperatures mainly, while the valancy, coordination, and nucleation of Co are less important.[38] The Al^{3+} ion polarizes the covalent Co−O bonds, resulting in an increase in the effective charge of the Co ions.[39] As a consequence, the lattice energy increases resulting in an increase in the TPR reduction temperatures. The peaks become more intense and sharp on increasing the calcination temperature from 450 to 900 °C probably because of an increase in the concentration of $Co^{2+}-Al^{3+}$ like species as mentioned in the previous section. For the sample calcined at 1100 °C, the TPR peak in region I is completely absent. A relatively sharp and intense peak, which can be resolved into three peaks centering at 347, 382, and 410 °C, respectively is recorded. Since, the XRD of the sample showed the presence of a well-crystallized phase corresponding to a solid solution, $Co^{2+}Al_{2-x}Co^{3+}_xO_4$ with $x \approx 1.326$, this peak can be attributed to the reduction of $Co^{2+}-Co^{3+}$ species diluted by Al^{3+}.

Region II (TPR Peak between 500 and 550 °C). CoAl-LDH calcined at 700 °C exhibits a shoulder (clearly seen in the deconvoluted curve) at 512 °C with a contribution of about 23% to the total Co species. On further calcination to 900 °C, the concentration of this species decreases to about 4% while it is almost absent in the sample calcined at 450 °C. These results indicate that there is possibly another Co-containing species existing which might be slightly different from both the $Co^{2+}-Co^{3+}$ species reduced in region I and $Co^{2+}-Al^{3+}$ species reduced in region III. From our XRD and TPR data, it is clear that calcination of CoAl-LDH leads to a nonstoichimetric spinel which can be considered as a mixture of Co_3O_4 (Co-rich spinel) and $CoAl_2O_4$ (Al-rich spinel). At low calcination temperatures (up to around 450 °C), the Co-rich spinel should be the predominant one that is reduced in region I. On the other hand, at higher calcination temperatures (around 900 °C), the Al-rich spinel could be formed predominantly and that is reduced in region III. Then it is reasonable to state that the Co species reduced in region II would correspond to an intermediate between Co-rich and Al-rich spinels. In other words, the Co species that is reduced in region II could be either Co_3O_4-like species containing Al^{3+} or $CoAl_2O_4$-like species containing Co^{3+}, which on further calcination at 900 °C transforms into an Al-rich spinel. However, in an earlier TPR study[38] on the Co/Al_2O_3 system prepared by the coprecipitation followed by calcination at 650 °C, also observed a reduction peak in this region, and it has been assigned to the reduction of a novel $Co^{3+}-Al^{3+}$ mixed oxide of the formula Co_3-

(37) van Steen, E.; Sewell, G. S.; Makhothe, R. A.; Micklethwaite, C.; Manstein, H.; de Lange, M.; Connor, C. T. O. *J. Catal.* **1996**, *162*, 220.
(38) Arnoldy, P.; Moulijn, J. A. *J. Catal.* **1985**, *93*, 38.
(39) Kung, H. H. *J. Catal.* **1982**, *73*, 387.

AlO_6. Spectroscopic studies are currently in progress to further confirm the nature of the Co species present in these regions.

The TPR profiles of CoAlSn-LDH calcined at various temperatures (see Figure 7) also show at least three reduction regions as those of the non-Sn-incorporated analogues. However, the profiles are even more complex, especially in the reduction region III, above 550 °C. The temperature of the TPR peak in region I due to the reduction of $Co^{2+}-Co^{3+}$ species increases with increasing precalcination temperature. It is interesting to note that the reducibility of these species diminished upon Sn incorporation. This is in contrast to the results observed in the Ni-contining analogues wherein the reducibility of Ni^{2+} species is enhanced by the presence of Sn^{4+}. It should be recalled that the XRD data indicated the possibility of the isomorphous substitution of Sn^{4+} for Al^{3+} or Co^{3+} to form a nonstoichiometric spinel of the formula: $Co^{2+}Al_{2-(x+y)}Co^{3+}Sn^{4+}{}_yO_{4+(y/2)}$ or $Co^{2+}Co^{3+}{}_{2-(x+y)}Al_xSn^{4+}{}_yO_{4+(y/2)}$. Thus, the $Co^{2+}-Co^{3+}$ species, which are reduced in region I, would contain Sn^{4+} besides Al^{3+}, thereby increasing the reduction temperature because of the enhanced polarization of Co−O bonds. The TPR peaks corresponding to $Co^{2+}-Al^{3+}$ species, which are reduced in region III, are more intense. No other peak was recorded beyond 700 °C when the TPR experiment of some of the samples was extended up to 800 °C. This result implies that the reduction of Sn^{4+} also completed before 800 °C and would probably coincide with the reduction of the $Co^{2+}-Al^{3+}$ species in region III (above 550 °C). The peak corresponding to region II (500−550 °C) is noticeable in all the samples calcined from 450 to 900 °C, indicating the existence of similar Co_3O_4-like species containing Al^{3+} or $CoAl_2O_4$-like species containing Co^{3+} in these samples. Similar to the non-Sn-containing counterpart, the sample calcined at 1100 °C exhibits three component peaks centering at 347, 411, and 539 °C, respectively. The former two peaks are in the same range as that noticed in the non-Sn-containing counterpart due to the reduction of $Co^{2+}-Co^{3+}$ species diluted by both Al^{3+} and Sn^{4+}. The latter peak at 539 °C, which accounts for about 36% would then correspond to the reduction of $Sn^{4+} \rightarrow Sn^0$ in the nonstoichiometric spinel.

Conclusions

In the present study, a new series of Sn-incorporated M(II)Al-LDHs, where M(II) is Ni or Co, has been synthesized, and their structural and redox properties have been compared with their non-Sn-containing counterparts. Thermal decomposition of these synthetic analogues led to dissimilar products. The NiAlSn-LDH offered Sn-doped NiO up to 700 °C, while Sn crystallized out as SnO_2 in addition to the $NiO/NiAl_2O_4$ phases above 900 °C. In contrast, a nonstoichiometric Co-spinel having a formula; $Co^{2+}Al_{2-(x+y)}Co^{3+}{}_xSn^{4+}{}_yO_{4+y/2}$ or $Co^{2+}Co^{3+}{}_{2-(x+y)}Al_xSn^{4+}{}_yO_{4+y/2}$ could be formed during calcination of CoAlSn-LDH up to 700 °C. Above this temperature, in addition to the nonstoichiometric spinel, an alumina-doped Co_2SnO_4 inverse spinel is obtained.

The reducibility of NiAl-LDH, CoAl-LDH, and their thermally derived products are greatly influenced by the Sn incorporation. For instance, the reducibility of both Ni- and Sn-containing phases is enhanced in the materials derived from Ni-containing LDH. This is probably because of the existence of an interaction between the Ni-containing phase and the SnO_2 phase formed in situ in these samples. In contrast, the reducibility of Co and Sn decreased in the materials derived from Co-containing analogues, and the result has been attributed to an enhancement in the polarization of Co−O bond due to the incorporation of Sn^{4+} in the Co-containing nonstoichiometric spinel lattice.

Three distinct H_2 reduction regions have been noticed in the Co-containing materials. On the basis of our XRD and TPR data, they have been assigned to the reduction of $Co^{2+}-Co^{3+}$ (Co_3O_4-like) species in region I (250−450 °C), Co_3O_4-like species containing Al^{3+} or $CoAl_2O_4$-like species containing Co^{3+} in region II (between 450 and 550 °C), and $Co^{2+}-Al^{3+}$ ($CoAl_2O_4$-like) species in region III (above 550 °C).

Acknowledgment. The authors S.V. and M.P.K. express their gratitude to the Japan International Science and Technology Exchange center (JISTEC) for the award of STA fellowships.

CM9904685